Effects of water absorption on the mechanical properties of GFRPs

Gustavo Quino[1], *Vito L. Tagarielli*[2,1*], *Nik Petrinic*[1]

[1]Department of Engineering Science, University of Oxford, OX1 3PJ Oxford, UK

[2]Department of Aeronautics, Imperial College, London, SW5 2AZ London, UK

Abstract

This study reports on the effects of water absorption on the anisotropic mechanical response of an epoxy resin reinforced with E-glass fibres. Composite specimens were conditioned by immersion in pure water at 50ºC for different time durations, up to full saturation. Water-saturation resulted in reduction of stiffness and strength, in the range of strain rate $0.001-700s^{-1}$. Experiments on re-dried specimens after water saturation showed only a small recoverability of the original mechanical properties. Water absorption increased the sensitivity of the mechanical response of the GFRPs to the applied strain rate. Finite element simulations of the response of a unit cell of the unidirectional composite were performed to understand the role of the hygroscopic stresses induced by water absorption, and it was found that this is negligible due to the active mechanisms of viscoelastic relaxation.

Keywords: composites; GFRP; epoxy; hygrothermal aging; strain rate sensitivity; viscoelasticity.

Submitted to Composites Science and Technology, November 2019

1. Introduction

Water exposure represents a very important challenge for marine composites. Previous research found that water absorption can affect the mechanical performance of laminated composites. For instance, it can decrease their strength [1], their interlaminar shear strength [2], [3], their flexural strength [4], their modulus [5], and affect their impact response [6]. Because of practical reasons, realistic immersion times of several years cannot be replicated in the laboratory; therefore, acceleration of water absorption is commonly forced by immersing composites in a water bath at elevated temperature [7]. However, care must be taken when selecting this temperature because too high temperatures may trigger mechanisms that would not appear under in-service conditions.

Experimental data in the literature shows that water diffusion in composites depends on the material, on the shape of the specimens and on the details of water immersion. For instance, water diffusion in composites has been reported to be Fickian [1], [3], [8] or non Fickian [9], [10]. Moreover, while some studies found that composites can be saturated with water [3], others show continuous weight increase [10] or even weight loss due to leaching of low weight molecules [7], [8], [11]. In composites with inorganic fibres, such as carbon and glass, water molecules can occupy voids, matrix-fibre interfaces [3], free volumes in the matrix [12] or chemically bond to the matrix [13].

The changes caused by water in the composite comes mainly from changes in the epoxy matrix [14]–[16] and damage of the fibre-matrix interface [17]–[20]. Some of these changes can be reversible (occupation of free volume) while others are non-reversible (chemical modification of the matrix or interface, micro-cracking, leaching). This means that some, but not all properties could be partially recovered after re-drying [2]. Micro-cracks can appear due to swelling or different thermal expansion coefficients between the matrix and fibre [7], [21].

Polymer-based composites are rate dependent, mainly due to the rate-dependent nature of the polymeric matrix. However, to the best of our knowledge, there is very little research into the influence of the water absorption upon the strain rate sensitivity of composites and it has been limited to compression specimens, with no study on the recoverability of mechanical properties after re-drying [6]. This study aims to fill this gap by exploring the material response in tension and in the three-point bending of short composite beams.

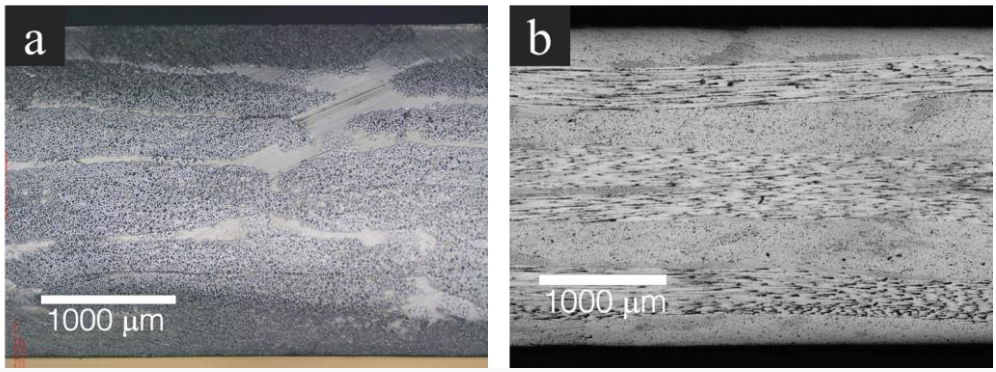


Figure 1. Optical micrographs of the microstructures of the GFRP plates tested, sectioned perpendicularly to the fibre direction. a) Unidirectional laminate, b) Bidirectional laminate.

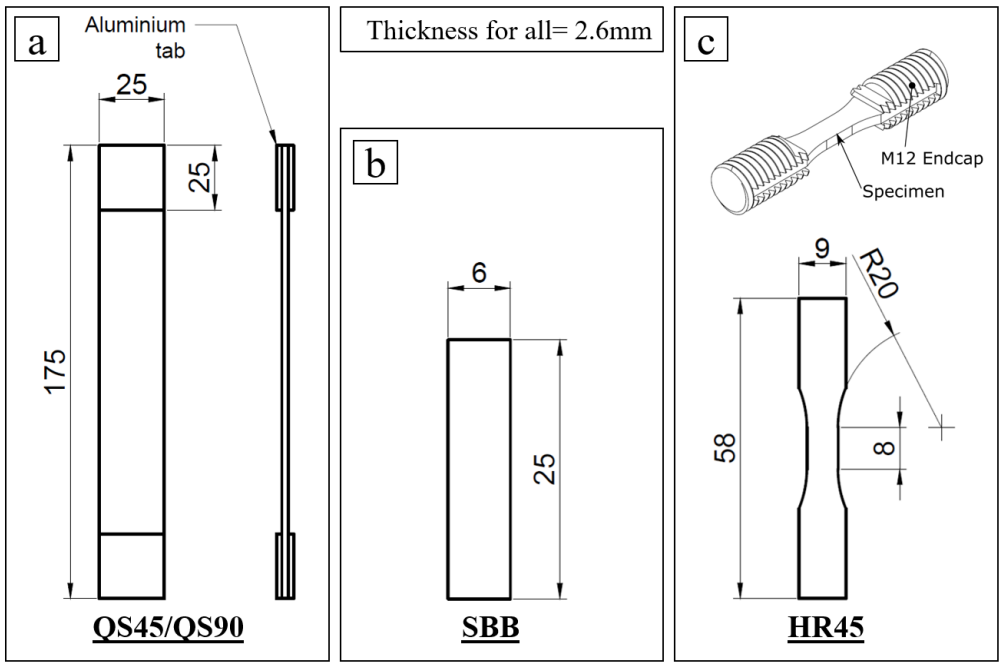


Figure 2. Geometry of the test specimens used in this study. a) quasi-static specimens QS90 and QS45; b) short beam specimens for 3-point bending (SBB); c) Hopkinson bar specimens (HR45).

It is accepted that water absorption induces swelling of the polymeric matrix [5], [7], [11], [22], [23], creating hygroscopic stresses within the composite matrix [24]. Derrien and Gilormini [24] developed analytical solutions for stresses induced by matrix swelling in the long term, neglecting viscous effects. Since during water absorption swelling and viscous relaxation occur simultaneously, we propose a method to evaluate the water-induced stresses that considers the competition between swelling and viscous relaxation of the matrix.

In the following Section we describe the experimental methods. Section 3 presents the modelling framework for the homogenisation and the swelling-viscoelastic relaxation analysis. Results are presented and discussed in Section 4.

2. Experimental methods

2.1. Materials and specimens

Specimens were machined from 600 × 600 × 2.6 mm^3 composites panels. The resin matrix in the composite was the Gurit Prime 20 ULV epoxy system. The reinforcement was the E-glass FGE238 non-woven unidirectional fabric, manufactured by Formax. This fabric contains 95%

of its areal weight of untwisted *tex* 1200 fibre bundles oriented in the 0° direction, and 5% of its aerial weight consists of untwisted *tex* 300 bundles on the 90° orientation. The bundles are stitched as a fabric with texturized polyester. Panels were prepared by resin transfer moulding (RTM), cured for 24 hours at room temperature and post-cured for 16 hours at 50°C. Panels with two stacking sequences were manufactured, $[0°]_8$ and $[90°, 0°]_{2s}$, with identical thickness and areal mass.

The volume fractions v_f of the unidirectional and bidirectional composites were calculated from their densities according to Equation (1).

$$v_f = \frac{\rho_c - \rho_r}{\rho_g - \rho_r}, \quad (1)$$

where ρ_c, ρ_r, ρ_g, are the densities of the composite, resin, and E-glass fibre, respectively. The densities of the resin and the composite were obtained from weight measurements (with 0.001 g precision) and knowledge of the volume of the specimens. The density of E-glass fibre ρ_g = 2.62 g/cm^3 was taken from literature [25].

The resulting values of v_f obtained by this method varied between 0.53 and 0.6 for both unidirectional and bidirectional specimens. This scatter is due to the uneven microscopic distribution of fibres and resin, especially in between the fibre fabrics and in between the bundles of the same fabric (see Figure 1). In the rest of the paper, an average volume fraction of 0.56 will be assumed.

For quasi-static (QS) characterisation, the following types of coupons were fabricated: $[90°]_8$ tensile specimens (labelled as QS90), $[45°]_8$ tensile specimens (labelled as QS45), and $[90°/0°]_{2s}$ short three point bending specimens (labelled as SBB). The tensile specimen orientations were chosen because they are expected to be particularly affected by changes in the mechanical properties of the epoxy matrix and of the fibre-matrix interface. In particular the 90° orientation maximises the tensile loading on this interface while the 45° orientation maximises shear loading. The choice of laminate layup was dictated by material availability, while SBB tests were selected to probe the interlaminar strength of the material. The QS90, QS45 and SBB specimens were manufactured by diamond saw cutting, with dimensions according to ASTM D3039 [26] and ASTM D2344 [27] (see Figures 2a and b). The axial response of the composites was not investigated as this is dominated by the response of the fibres, and preliminary experiments showed that the performance of the dry fibres is unaffected by water absorption.

For high strain-rate experiments, $[45^{\circ}]_8$ grinded dogbone tensile specimens were manufactured as illustrated in Figure 2c. Dogbone specimens were preferred because at high strain rates they exhibit consistent failure within the gauge section. The proposed geometry was found to be a good balance between having a specimen long enough to be representative of the material and short enough to provide with consistent force equilibrium and high strain rates. The two steel threaded shoulders glued to their ends allowed easy mounting to the split Hopkinson bar (Figure 2c).

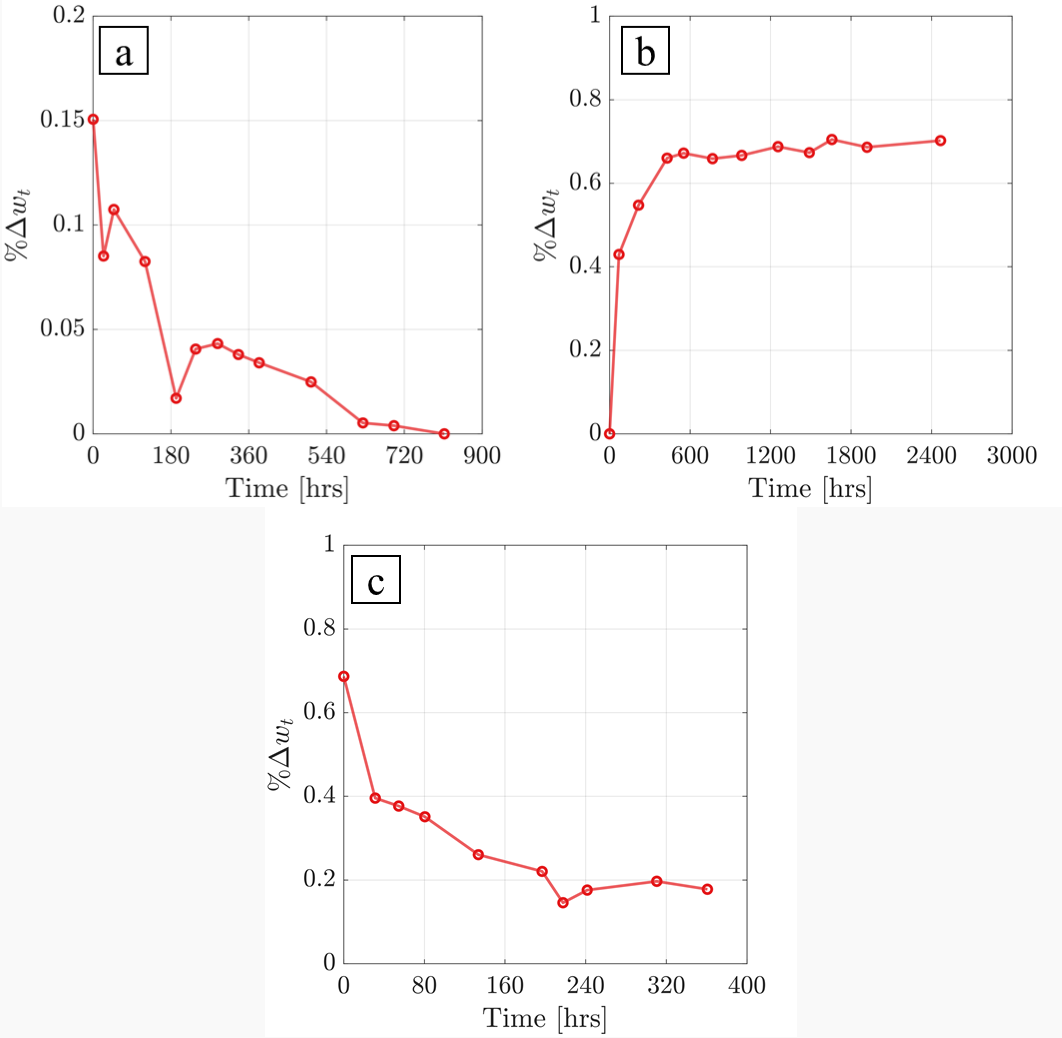


Figure 3. Time histories of the water content of the composite specimens during conditioning: a) drying cycle; b) water saturation cycle; c) re-drying cycle.

2.2. Water absorption

Specimens were conditioned by immersion in distilled water at 50ºC, well below the glass transition temperature of the epoxy matrix. This was measured from DMTA experiments as T_g = 79°C and was in line with that reported by the manufacturer (T_g = 81°C). The sides of the coupons were protected with adhesive aluminium tape to prevent diffusion in the direction normal to the sides [8], ensuring unidirectional through-thickness diffusion. Diffusion in the direction of the fibres may lead to capillarity effects [7] which here we want to eliminate. The gravimetric analysis was performed after removing the aluminium tape.

Samples were dried in a Binder FED series oven at 50°C prior to immersion in the water bath. The weight was periodically monitored with an OHAUS DV215 balance (0.01 mg precision), to determine the water intake history.

The measured weight was used to determine the percent water content $\%\Delta w_t$:

$$\%\Delta w_t = \frac{(w_t - w_{FD})}{w_{FD}} \times 100\% \quad (2)$$

where w_t is the weight at the monitoring time t, and w_{FD} is the weight of the fully dry specimen ($\%\Delta w_t = 0$). Complete drying was identified by the stabilisation of the water content, achieved after approximately 600 hours (Figure 3a). Fully dry specimens (FD) were tested to have a baseline value of the composite properties.

The dry specimens were later immersed in the water bath at 50ºC. Water absorption was again measured by Equation (2), reaching saturation after approximately 1200 hours, with a maximum percent water content of $\Delta w_s^{comp} = 0.71\%$ (Figure 3b). Saturated specimens (WS) were tested after a total of approximately 2500 hours of immersion, to observe the effects of water saturation.

To verify if the effects caused by water absorption were recoverable, fully saturated specimens were re-dried in the oven at 50°C until no significant change in weight was measured. Specimens reached this condition in approximately 300 hours (Figure 3c) and were identified with the label RD (water – re-dried).

In a similar study [28] on the same epoxy resin, absent the fibres, we measured the percent water content at resin saturation, $\%\Delta w_s^r$ = 2.81%. Upon assuming that the glass fibres do not absorb any water, it is possible to estimate the percent water content in the composite $\%\Delta w_s^{comp}$, using simple rule-of-mixtures. For the range of fibre volume fractions in our composite specimens (v_f = ⟦0.53; 0.60⟧) we predict a percent water content in the composite

in the range ⟦0.63; 0.78⟧%. This is consistent with the values which we directly measured, confirming that the hypothesis of glass fibres absorbing negligible water may be acceptable. This hypothesis was further substantiated by preliminary measurements of water absorption on the dry glass fabric, which showed negligible water intake over the same time period (2500 hours) of exposure of the composites.

2.3. Mechanical characterisation

All tests were performed in the lab conditions with 40±8% relative humidity and at 20±2°C. Specimens were removed from their conditioning bath and prepared for testing in under 25 minutes. This time was sufficiently long to reach thermal equilibrium and sufficiently short to prevent significant loss or gain of moisture.

In the quasi-static regime, all tests were performed in a Zwick Z250 screw-driven universal testing machine. QS90 and QS45 specimens were tested following the recommendations of ASTM D3039 [26]. The specimens were clamped from their aluminium end tabs with wedge grips moving at a prescribed relative displacement rate of 0.0125 mm/s. The force was measured with a load cell of capacity 250 kN, while the strains were obtained from DIC analysis of footage, recorded by a JAI camera at 1 fps.

The bending tests on SBB specimens followed the recommendations in ASTM D2344 [27]. The specimens were supported by two rollers of 1.5 mm radius, with a span length of 12.5 mm. The load was applied at mid-span by a roller of 3 mm radius moving at a speed of 0.0166 mm/s. The applied force was measured by a load cell of capacity 20 kN. The displacements of the midpoint were computed from the DIC as described above. The strength τ_u of the SBB specimens was calculated from the measured peak force P_m

$$\tau_u = 0.75 \cdot \frac{P_m}{b \cdot h} \quad (3)$$

where b and h are the width and thickness of the specimen respectively. Note that the above equation is consistent with the assumption of interlaminar shear failure at mid-thickness during the test, which was the observed mechanism in all tests.

At high strain rates, dogbone specimens were tested in the split Hopkinson pressure bar, with a configuration as described in [29]–[31]. The stress versus time history was calculated with one-dimensional wave theory, using the measurements from three sets of strain gauges. Appendix A describes in more detail the Hopkinson bar and the procedure to find the history

of loads. The history of axial strain was measured via DIC analysis using the commercial software GOM Aramis (GOM UK Ltd). Pictures were taken at 200000 fps by a Kirana camera (Specialised Imaging Ltd, UK) with a resolution of 924x768 pixels. Force equilibrium of the specimen was obtained after approximately 700 μs, after which the strain rate was approximately constant.

At least three repetitions were conducted for all types of tests. Table 1 presents the test matrix, summarising the types of tests, conditioning environments, and the labels that will be used to identify each test.

Table 1: Labelling of different specimens and conditioning for the composite materials tested in this study.

Specimen\Conditioning	**FD (fully dried)**	**WS (water-saturated)**	**RD (re-dried)**
QS45 (off-axis 45°)	QS45-FD	QS45-WS	QS45-RD
QS90 (transverse 90°)	QS90-FD	QS90-WS	QS90-RD
HR45 (off-axis 45°)	HR45-FD	HR45-WS	HR45-RD
SBB (short beam – 3-point bending)	SBB-FD	SBB-WS	SBB-RD

Measurements of matrix swelling were also conducted using a neat resin specimen of dimensions $30 \times 50 \times 2.4\ \text{mm}^3$. Measurements with a micrometre (0.01 mm resolution) prior and after immersion showed an approximately linear, isotropic hygroscopic expansion, with hygroscopic strains proportional to the percent water content; the constant of proportionality was measured as 0.0023. At the maximum water content (recall that, at resin saturation, it was $\%\Delta w_s^r = 2.81\%$) this corresponded to a strain of 0.0066.

The viscoelastic properties of the matrix were characterised by DMTA on a $35 \times 10 \times 2.65\ \text{mm}^3$ neat resin specimen, tested in tension mode as described in [32]. The coupon was subjected to a frequency and temperature sweep from 0.001 to 30 Hz, and from 10-110°C in steps of 5°C.

3. Modelling framework

We performed a finite element (FE) analysis of a composite unit cell to study the homogenised material properties and the build-up of thermal and hygroscopic stresses in the composite specimens, and the effects of water absorption on the macroscopic stiffness of the composites. A cubic unit cell Ω of side length 1 and fibre volume fraction $v_f = 0.56$ was modelled as in Figure 4, consistent with cubic packing of the fibres in the matrix. The properties of resin and E-glass fibres, obtained from reference [28] and preliminary experiments, were used to calibrate the constitutive models for fibres and matrix. For the resin, the elastic moduli used were $E_r^{FD} = 2.6$ GPa, $E_r^{WS} = 2.0$ GPa, $E_r^{RD} = 2.4$ GPa; and the corresponding Poisson's ratios were $\nu_r^{FD} = \nu_r^{WS} = \nu_r^{RD} = 0.4$. The properties of the E-glass fibres were taken to be independent from water content: $E_g = 60$ GPa (directly measured) and Poisson's ratio $\nu_g = 0.18$ taken from literature [33]. 3D solid elements with linear shape functions were used for all simulations.

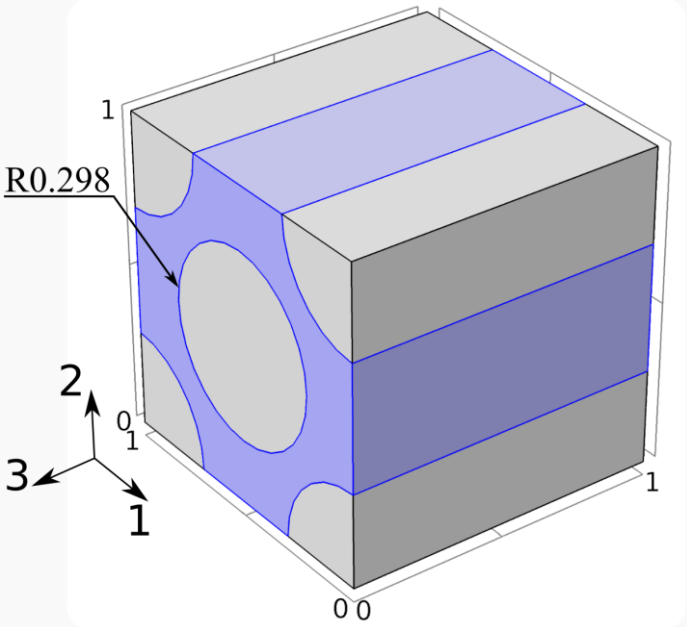


Figure 4. Geometry of the cubic unit cell used in the FE simulations and corresponding reference system.

3.1. Homogenised elastic properties

The elastic properties of the lamina were calculated running a series of simulations in COMSOL Multiphysics v4.4 [34] using the implicit solver, using tetrahedral elements with average element size of 0.03. Periodic boundary conditions were prescribed on opposite faces of the cubic unit cell; homogenised strains and stresses were obtained from the degrees of freedom of appropriate auxiliary nodes. When analysing the elastic properties, the unit displacement method was used to populate the homogenised stiffness matrix of the composite [32], [35], [36], obtaining the lamina constants E_3, E_2, G_{12}, ν_{12}, ν_{23}. The material was taken as initially stress-free, based on the results of simulations described below.

3.2. Matrix swelling

We assume that as water diffuses into the composite it induces swelling of the matrix but not of the glass. Hygroscopic expansion induces only direct strains, but no shear strains, on unconstrained components made from the epoxy resin; this phenomenon is analogous to thermal expansion and it was modelled in Abaqus v6.14 [37] as a thermal expansion, following appropriate redefinition of the physical variables. The mismatch in hygroscopic strains leads to the build-up of tri-axial stresses in the composite, which can be evaluated by FE analysis.

3.3. Matrix viscoelasticity

The DMTA measurements of storage and loss Young's moduli (E' and E'' respectively) were post-processed using the time-temperature equivalence method described in [38], allowing the construction of a master curve. We assumed that the resin's Poisson's ratio was real and independent of frequency, following [35], leading to:

$$G^* = \frac{E^*}{2(1+\nu)} \quad (4)$$

$$K^* = \frac{E^*}{3(1-2\nu)} \quad (5)$$

where * indicates a complex number, e.g. $E^*=E'+i\,E''$ (where i is the imaginary unit). The viscoelastic material behaviour was modelled in Abaqus/Standard providing Prony series of the real and imaginary parts of the shear and bulk moduli. Prony coefficients and long-term bulk and shear moduli were determined from experiments as in [35]. The geometry was identical to that described in Section 3.1 and was meshed using element type C3D8R and

average element size of 0.02. Four simulation cases were considered to explore the effects of the viscoelastic relaxation:

a) instantaneous matrix swelling (corresponding to full saturation) followed by viscous relaxation for 2800 hours;
b) simultaneous matrix swelling and viscous relaxation for 500 hours, followed by viscous relaxation 2300 hours;
c) simultaneous matrix swelling and viscous relaxation for 1000 hours, followed by viscous relaxation 1800 hours;
d) simultaneous matrix swelling and viscous relaxation for 2800 hours.

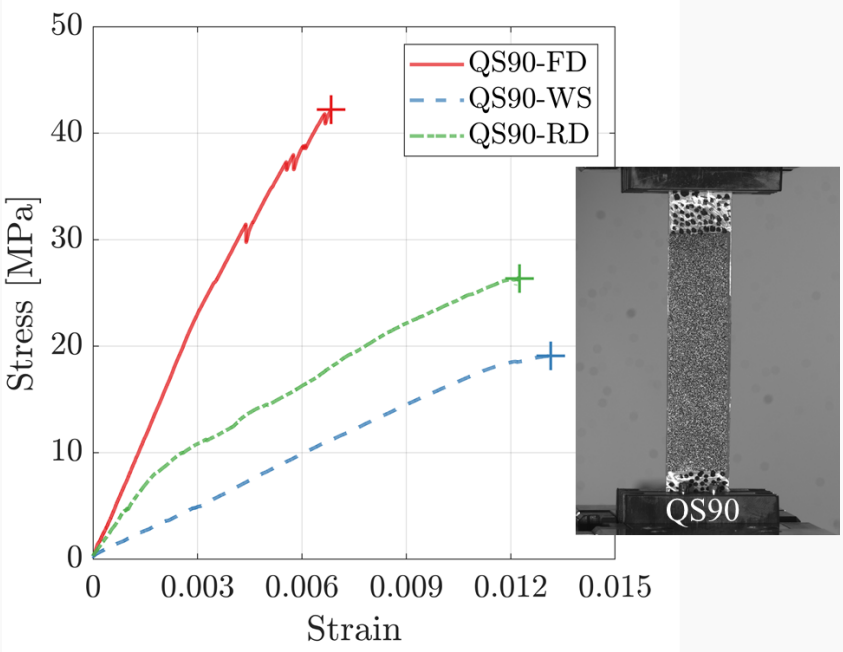


Figure 5. Representative stress versus strain histories for the QS90 tests. The crosses indicate the point of ultimate failure.

4. Results and discussion

We proceed to present and discuss the results from the present study. Results are displayed according the label scheme introduced in Table 1. In some cases, the number at the end of the label indicates the strain rate of the test in s^{-1}.

4.1. Effects of conditioning on the mechanical response

Figure 5 shows typical strain versus stress curves observed in QS90 tests, for all three conditioning cases. Figure 6 displays representative strain versus stress curves of experiments on QS45 and HR45 specimens at all conditioning environments. In both QS45 and QS90 tests, there is a linear region at the beginning of the curve, where the Young's modulus E is measured. Note that the modulus was not extracted from high strain rate tests, as in the initial part of the strain-stress curve the specimen is not in force equilibrium; however, equilibrium is reached before the peak stress, which allows extracting the dynamic strength of the specimens.

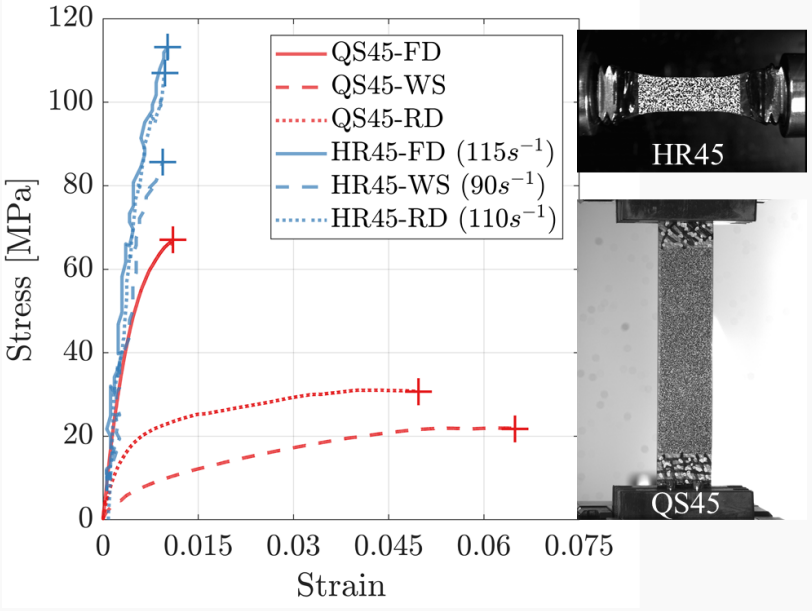


Figure 6. Representative stress versus strain histories for the off-axis uni-directional specimens, for quasi-static (QS45) and dynamic (HR45) loading conditions. The crosses indicate the point of ultimate failure.

Figure 7 displays representative force versus displacement curves measured in the short-beam bending tests. After an initial elastic response, a maximum load P_m is attained, followed by softening induced by the observed shear-driven damage and inelastic deformation of the matrix.

Figure 8a and Figure 8c show the effects of the conditioning procedures upon the Young's modulus E of QS90 and QS45 specimens. The homogenised elastic modulus obtained by the FE simulations described in Section 3.1 are included for comparison. Figure 8b and Figure 8d display the strengths σ_u of QS90 and QS45 specimens, respectively. The graphs

include the measured strengths of the neat resin for comparison. Figure 9 presents the fracture surfaces of the specimens tested at high strain rate, while Figure 10 summarises the effects of water saturation and re-drying upon the short beam strength τ_u obtained in the SBB tests.

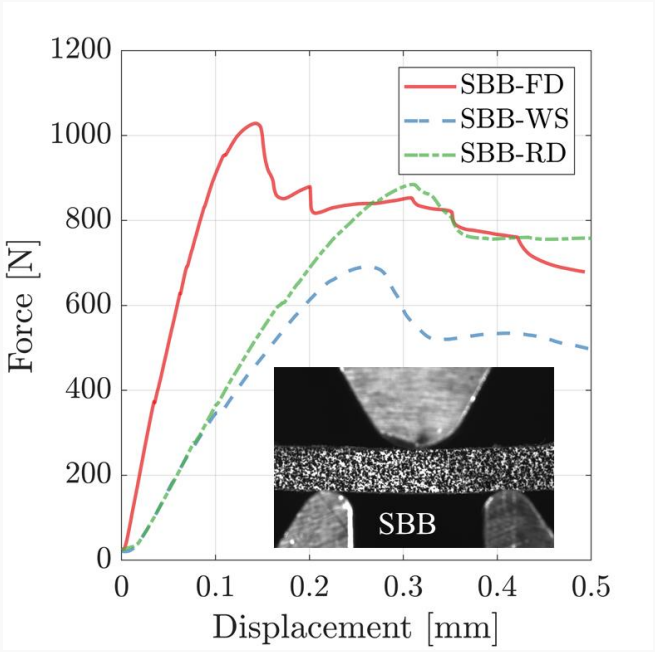


Figure 7. Representative force versus mid-span deflection histories measured in the 3-point bending tests on SBB composite specimens.

Figure 11 shows the influence of the imposed strain rate and of the conditioning procedures upon the tensile strengths of QS45 and HR45 coupons. The figure includes best fits of the measured data by power-law expressions, and the corresponding exponents and multipliers of these power-law fits are presented in Table 2.

Table 2: Resulting parameters of fitting the QS45 and HR45 strengths to the power law $\sigma_u = A\dot{\varepsilon}^n$.

Parameter\Conditioning	**FD**	**WS**	**RD**
A	89.1	51.9	59.8
n	0.049	0.108	0.095

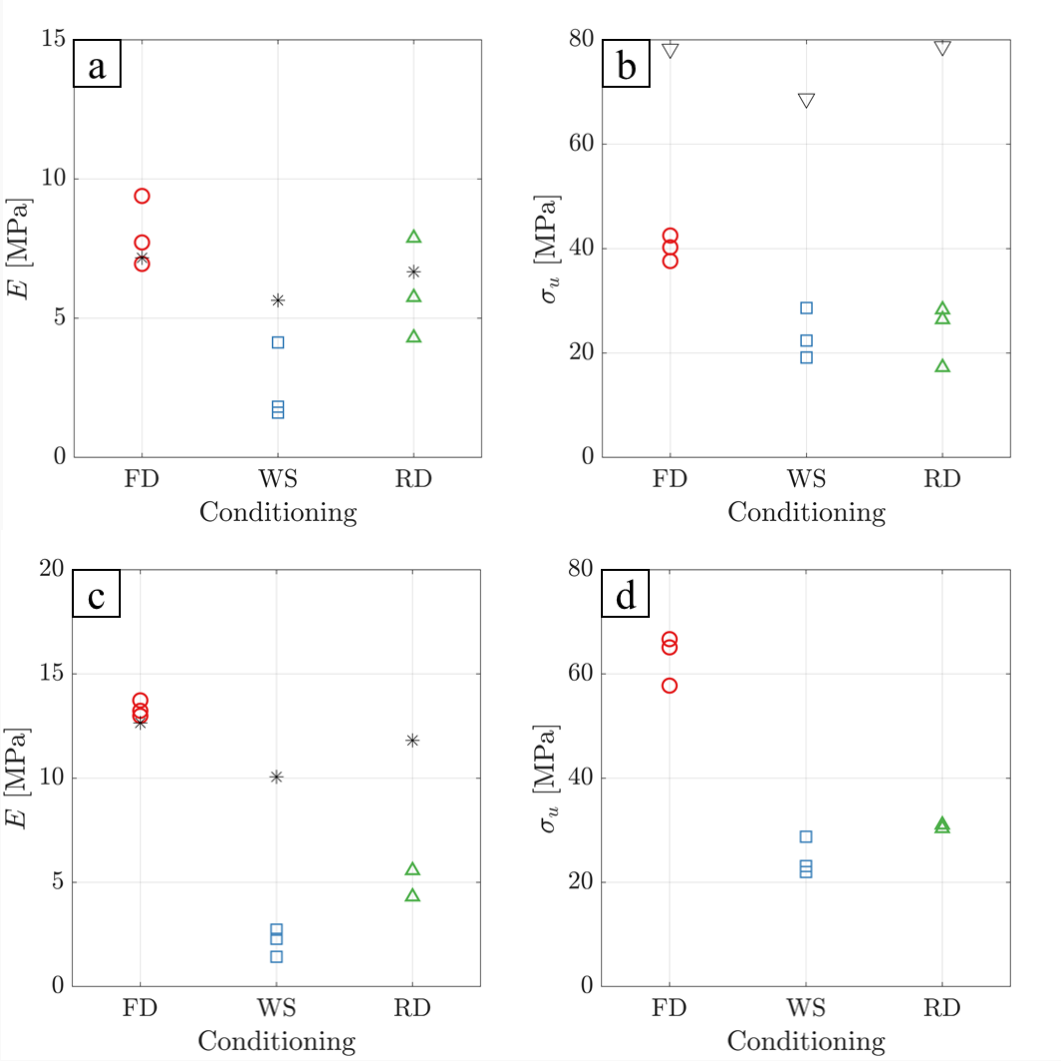


Figure 8. Sensitivity of the measured quasi-static stiffness and strength of the composite specimens to the three types of conditioning (FD ○, WS □, RD △). a), b): QS90 specimens; c), d): QS45 specimens. a) and c) include FE predictions (∗); b) includes the measured strengths of the neat resin measured in [28] (∇).

We found that water absorption caused detrimental effects on the mechanical response of the composites, for all tests and at all strain rates explored (Figures 5-8,10). The tensile strength, elastic modulus, and interlaminar shear strength decreased when composites were fully saturated with water, in contrast with what reported in [6], in which composites were tested in compression.

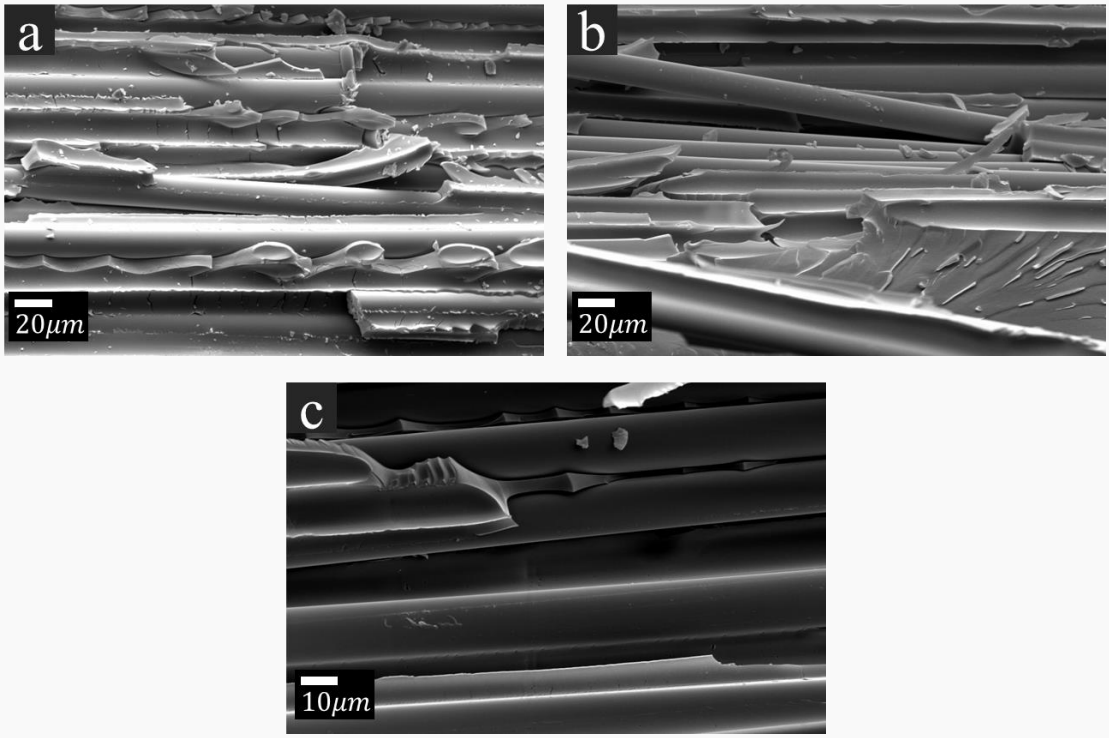


Figure 9. Effect of the three different types of conditioning on the fracture surfaces of the HR45 specimens. Details of the fibre-matrix interfaces are shown via high-magnification SEM images. a) FD, b) WS, c) RD.

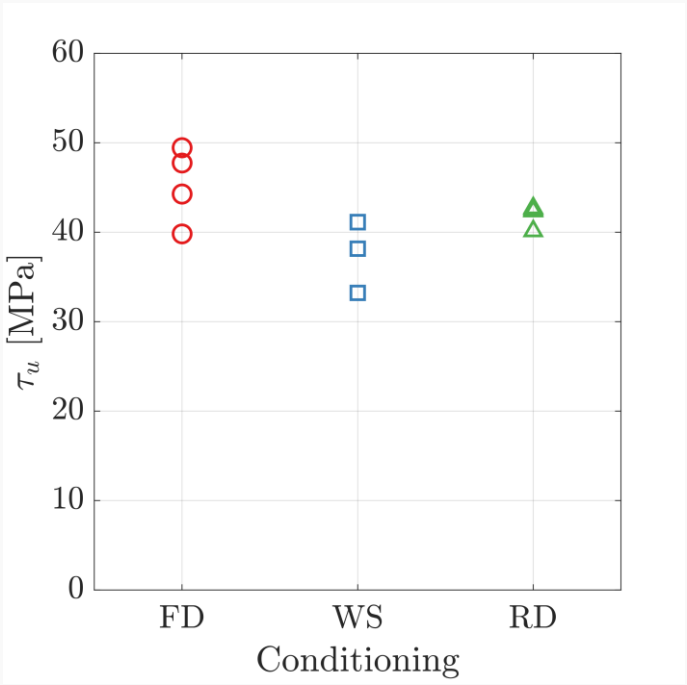


Figure 10. Sensitivity of the measured quasi-static interlaminar shear strength of the multidirectional composite specimens to the three types of conditioning (FD ○, WS □, RD △).

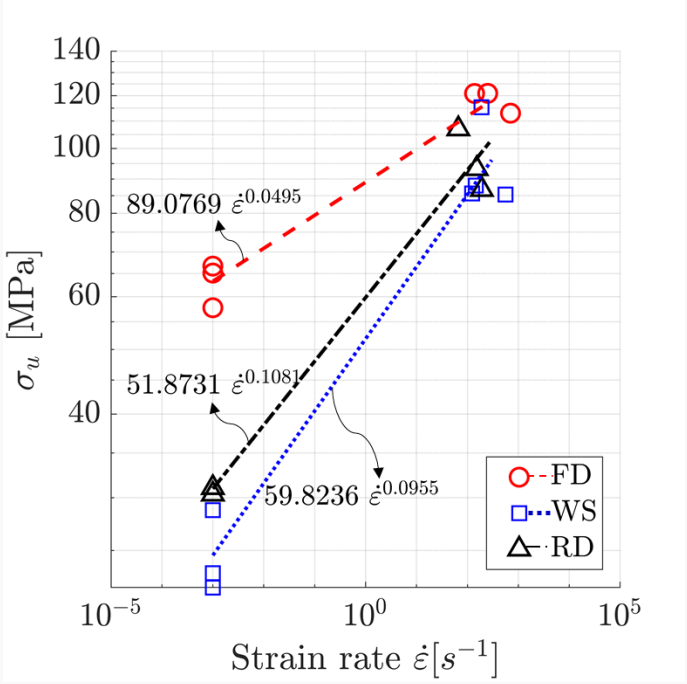
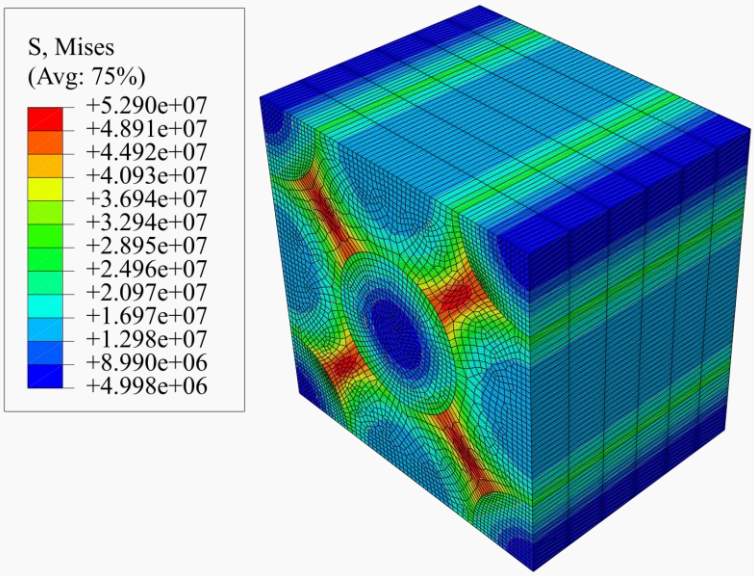


Figure 11. Measured strain rate sensitivity of the off-axis specimens QS45 and HR45. The figure includes power-law best fits through the measured data.

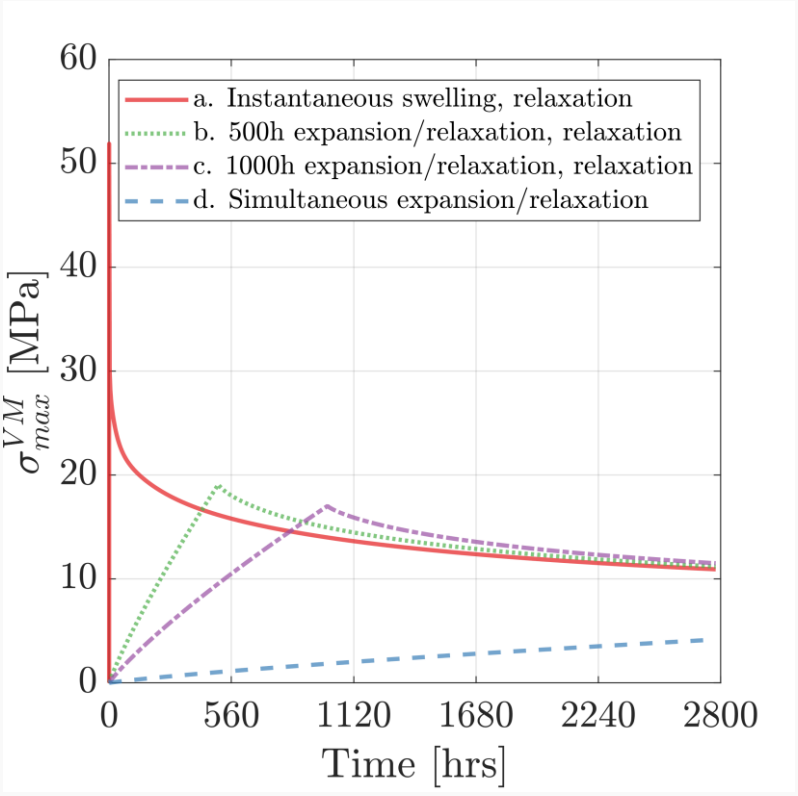
Water exposure reduced the Young's modulus by 80%, and the strength by 50% on QS90 specimens, while reductions were of 80% and 58% (on E and σ_u, respectively) for QS45 specimens. QS90-WS and QS45-WS specimens (Figures 6,7) showed a higher strain to failure than fully dry specimens, in line with the slight increase in ductility of the matrix which we measured in [28].

The tests conducted on re-dried specimens show that in all cases re-drying allows only partial recovery of the stiffness and strength of the material and of the interlaminar interface.

With focus on Figure 8a and Figure 8c we note that our FE simulations, which assume no deterioration of the fibre-matrix interface, are in agreement with measurements for the case of fully dried specimens. However, the simulations over predict the modulus of water-saturated and re-dried specimens. These results further support the idea of water weakening the fibre-matrix interface [39], and that such weakening is more pronounced for shear loading of such interfaces.



348
349
350 Figure 12. Simulated contours of von Mises stresses consequent to hygroscopic matrix
351 swelling, absent viscoelastic relaxation. Maximum Von Mises stress: $\sigma_{max}^{VM} = 52.9$ MPa.



352
353 Figure 13. Time history of the predicted maximum von Misses stress in the unit cell, for the
354 four load cases a, b, c, d described in Section 3.3.

355
356 Now focus on Figure 8b and Figure 8d: the strength of the QS90 specimens is, as
357 expected, lower than the strength of the neat resin, due to the stress concentration induced by

the presence of the fibres. While the measurements in [28] suggested that the strength of the matrix could be highly recoverable upon re-drying, for the composite this is not the case. This reinforces the notion that the fibre-matrix interface strength is permanently weakened by water absorption. The effects of water absorption on the strength of the QS90 specimens (matrix-dominated) would be expected to be similar to the reduction in strength of the neat resin (12% drop); however, such drop in strength is more pronounced in the composite specimens (50%), again in line with weakening of the interfaces. The analysis of fracture surfaces provides some insight on the different failure mechanisms induced by water absorption. Fracture surfaces of HR45 specimens, obtained by SEM imaging for all three conditioning procedures explored in this paper, are shown in Figure 9. Smoother resin areas are seen for water-saturated and re-dried specimens, while rougher fracture surfaces are observed for the fully dry material. This might suggest a more ductile behaviour in this case, however this should be substantiated by further fractographic analysis.

Figures 7 and 10 show that water absorption also weakens substantially the interlaminar shear strength of the composites, and that this weakening cannot be fully removed upon re-drying of the specimens. Figure 11 shows that the composite is rate sensitive regardless of the conditioning of the specimens. The drop in strength FD to WS however is not the same at different strain rates (58% for 0.001 s^{-1}, and 30% for 100 s^{-1}). This suggests that the material seems to be less affected by water degradation at higher strain rates; this is the same trend that was observed by the authors for the neat resin [28] and results in higher strain rate sensitivity on conditioned specimens with respect to dry specimens, as confirmed by the higher exponents *n* in the power laws (Table 2). Therefore, the changes in strain rate sensitivity of the composite are mainly driven by the changes in the strain rate sensitivity of the epoxy matrix.

4.2. Combined effects of hygrothermal stresses and viscous relaxation

Figure 12 shows the resulting Von Misses stress field obtained from FE simulations, following loading by hygroscopic straining, corresponding to the water content at full saturation, absent any relaxation mechanisms. The maximum Von Mises σ_{max}^{VM} stress is experienced in the matrix and reaches a value of 52.9 MPa. This value has to be considered as an upper bound, as simulations were conducted with a constant value of the modulus of the matrix (equal to the modulus of the fully dried resin – the highest possible), while we have shown in [29] that the

modulus can decrease by a factor of approximately 25%, which would lead to a corresponding decrease in the maximum hygroscopic stresses of order 25%.

Figure 13 shows how such maximum stress σ_{max}^{VM} is attenuated when viscoelastic relaxation is considered, together with a finite time for water absorption and the associated hygroscopic straining. In the case where hygroscopic straining and viscoelastic relaxation occur simultaneously over time (loading case d), the resulting maximum stress is of less than 5 MPa. Considering that simulations do not account for the decrease in the modulus of the matrix, and that in realistic scenarios the time scales for water saturation are much longer than the 2800 hours considered in our simulations, we conclude that the role of residual hygroscopic stresses is negligible in determining the macroscopic strength of composites subject to water absorption.

We noted above that at saturation the matrix displays a free hygroscopic strain of 0.0066. Considering that the coefficient of thermal expansion of epoxies is of order 10^{-4} K^{-1}, a temperature difference of order 66 K would be needed to induce a similar strain in the matrix. We also note that the coefficient of thermal expansion of glass fibres is or order 10^{-6} K^{-1}, much lower than that of the matrix. We deduce that similar results as those in Figures 12 and 13, obtained with hygroscopic expansion in mind, would be obtained modelling the build–up of thermal stresses upon cooling from the curing or post-curing temperature, as well as those arising from heating during the conditioning process. This justifies the assumption, made in Section 3.1, of an initially stress-free composite microstructure.

5. Conclusions

An experimental testing campaign and accompanying FE simulations were conducted to unveil and understand the effects of water absorption upon the mechanical response of GFRPs for marine applications and their sensitivity to strain rate. The main conclusions of this paper are as follows:

- Water absorption reduced the stiffness and tensile strength of uni-directional composites as well as the interlaminar shear strength of multi-directional composites, at all strain rates investigated. This is consequent to a decrease in modulus and strength of the matrix, as well as the weakening of the fibre-matrix and interlaminar interfaces.
- Water absorption slightly increases the ductility of the composites in matrix-governed loading cases, consequent to the increase in ductility of the matrix.

- Re-drying of GFRPs after full water saturation cannot eliminate all the water absorbed and allows only a partial recovery of the original properties of the composites.
- Water-saturated composites have higher strain rate sensitivity than fully dried composites.
- The role of hygrothermal stresses is negligible in determining the deterioration of the mechanical properties due to the presence of viscoelastic relaxation mechanisms.

Acknowledgements

This project was supported by EPSRC, [dstl] and Rolls-Royce plc [grant EP/G042586/1].

Appendix A

In this Appendix we describe the Hopkinson bar system and the calculation of the history of forces *F(t)* acting upon the specimen during the experiment. In the Hopkinson bar system, a stress wave is generated by the impact of a projectile. The wave travels through the input bar, specimen and output bar. The waves is transmitted and partially reflected at each interface. Figure A1 shows the schematic of the system and the associated forward and backwards, respectively α and β, waves in the input (superscript *I*) and output (superscript *O*) bars. One-dimensional wave analysis gives the stresses, at the location x_{G_i} of the strain gauges can be calculated from their measured strains as:

$$\sigma\left(x_{G_i}, t\right) = \varepsilon\left(x_{G_i}, t\right)E_b, \tag{A.1}$$

where E_b is the elastic modulus of the bar. The alpha and beta waves are calculated at the end of the input bar x_e^I and the beginning of the output bar x_b^O over the time domain (refer to Figure A1 for the meaning of each t_i):

$$t < t_4 \begin{cases} \alpha(x_e^I, t) = \sigma\left[x_{G_1}^I, t - (t_3 - t_1)\right] \\ \beta(x_e^I, t) = \sigma\left[x_{G_2}^I, t + (t_3 - t_2)\right] - \sigma\left[x_{G_1}^I, t + (t_3 - t_2) - (t_2 - t_1)\right] \end{cases} \tag{A.2}$$

$$t_4 \le t \begin{cases} \alpha(x_e^I, t) = \sigma\left[x_{G_1}^I, t - (t_3 - t_1)\right] - \beta[x_e^I, t - (t_4 - t_3)] \\ \beta(x_e^I, t) = \sigma\left[x_{G_2}^I, t + (t_3 - t_2)\right] - \{\sigma\left[x_{G_1}^I, t + (t_3 - t_2) - (t_2 - t_1)\right] - \beta[x_e^I, t - 2(t_2 - t_1)]\} \end{cases} \tag{A.3}$$

$$t < t_7 \begin{cases} \alpha(x_b^O, t) = \sigma\left[x_{G_3}^O, t + (t_6 - t_5)\right] \\ \beta(x_b^O, t) = 0 \end{cases} \tag{A.4}$$

$$t_7 \le t < t_8 \begin{cases} \alpha(x_b^O, t) = \sigma\left[x_{G_3}^O, t + (t_6 - t_5)\right] + \alpha[x_b^O, t - (t_7 - t_5)] \\ \beta(x_b^O, t) = 0 \end{cases} \tag{A.5}$$

$$t_8 \le t \begin{cases} \alpha(x_b^O, t) = \sigma\left[x_{G_3}^O, t + (t_6 - t_5)\right] + \alpha[x_b^O, t - (t_7 - t_5)] \\ \beta(x_b^O, t) = -\alpha[x_b^O, t - (t_8 - t_5)] \end{cases} \tag{A.6}$$

The force history upon the specimen is then evaluated as

$$F(t) = \frac{1}{2}\{A^I[\alpha(x_e^I, t) + \beta(x_e^I, t)] + A^O[\alpha(x_b^O, t) + \beta(x_b^O, t)]\}, \tag{A.7}$$

where A^I and A^O are the cross sectional areas of the input and output bar respectively.

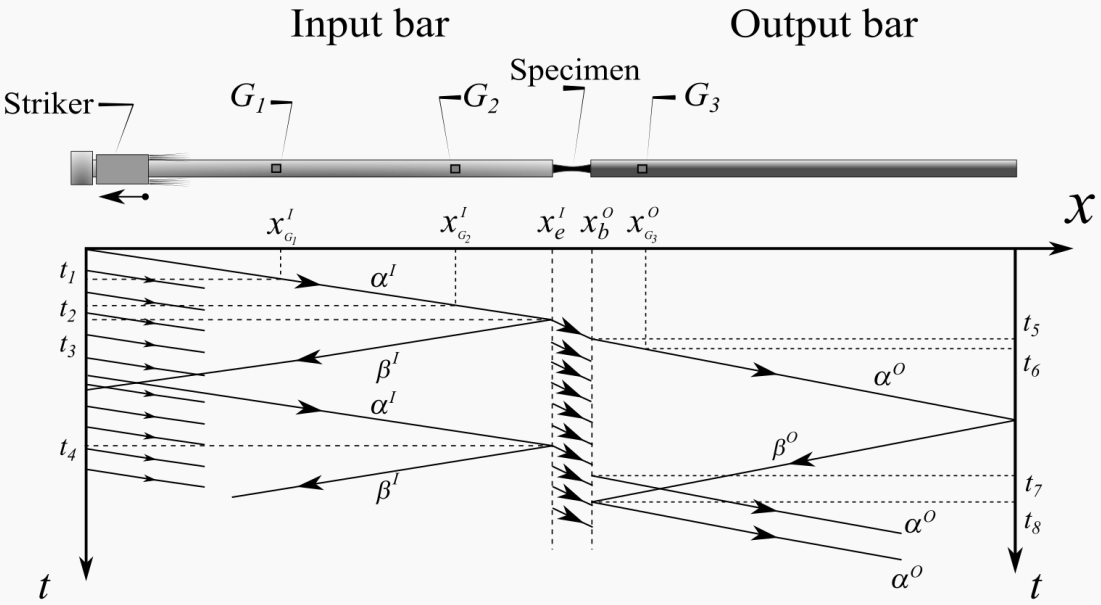


Figure A1. Schematic of Split Hopkinson bar showing locations of strain gauges and history of forward (α) and backwards (β) solid waves along input and output bar.

Appendix B

In this Appendix we provide the raw DMTA measurements of storage and loss moduli, shown in Figures B1a and B1b, respectively. Figures B1c and B1d display the master curves for the storage and loss moduli constructed from the raw data, using a reference temperature of 50°C.

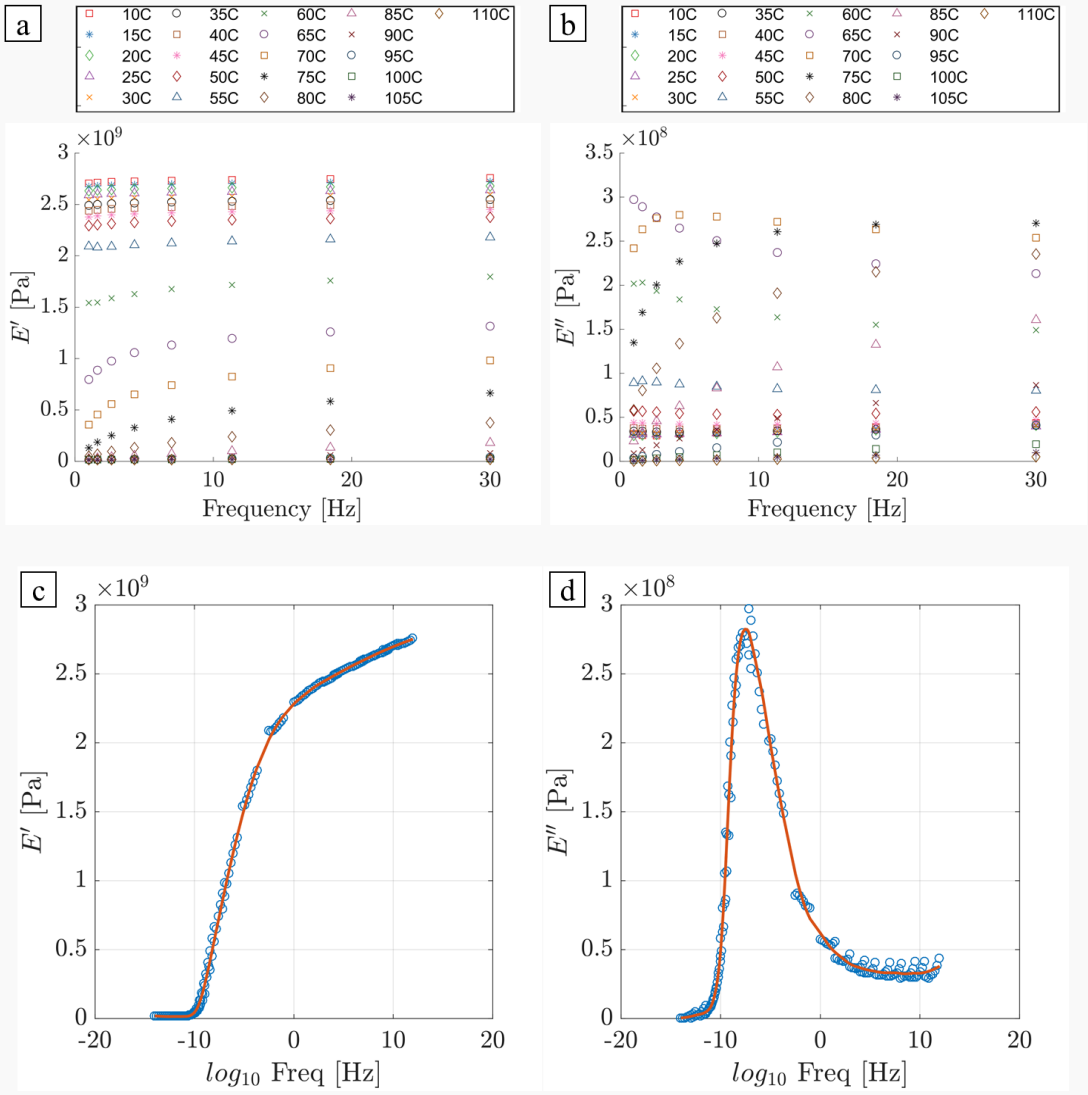


Figure A2. Raw data from DMTA measurements on the neat resin specimens and the corresponding processed master curves. a) Storage modulus as a function of temperature and frequency; b) Loss modulus as a function of temperature and frequency; c) Master curve for the storage modulus; d) Master curve for the loss modulus.

References

[1] A. Avena and A. R. Bunsell, "Effect of hydrostatic pressure on the water absorption of glass fibre-reinforced epoxy resin," *Composites*, vol. 19, no. 5, pp. 355–357, Sep. 1988.

[2] L. Bian, J. Xiao, J. Zeng, and S. Xing, "Effects of seawater immersion on water absorption and mechanical properties of GFRP composites," *J. Compos. Mater.*, vol. 46, no. 25, pp. 3151–3162, Feb. 2012.

[3] E. P. Gellert and D. M. Turley, "Seawater immersion ageing of glass-fibre reinforced polymer laminates for marine applications," *Compos. Part A Appl. Sci. Manuf.*, vol. 30, no. 11, pp. 1259–1265, Nov. 1999.

[4] G. Steinbrecher, B. Cohen, and E. Altus, "Hygromechanical coupling in laminate composites and its effect on interlaminar failure," *Compos. Part A Appl. Sci. Manuf.*, vol. 84, pp. 123–133, May 2016.

[5] S. Aldajah, G. Alawsi, and S. A. Rahmaan, "Impact of sea and tap water exposure on the durability of GFRP laminates," *Mater. Des.*, vol. 30, no. 5, pp. 1835–1840, May 2009.

[6] E. Woldesenbet, N. Gupta, and J. R. Vinson, "Determination of moisture effects on impact properties of composite materials," *J. Mater. Sci.*, vol. 37, no. 13, pp. 2693–2698, 2002.

[7] B. Dewimille and A. R. Bunsell, "Accelerated ageing of a glass fibre-reinforced epoxy resin in water," *Composites*, vol. 14, no. 1, pp. 35–40, 1983.

[8] S. A. Grammatikos, B. Zafari, M. C. Evernden, J. T. Mottram, and J. M. Mitchels, "Moisture uptake characteristics of a pultruded fibre reinforced polymer flat sheet subjected to hot/wet aging," *Polym. Degrad. Stab.*, vol. 121, pp. 407–419, Nov. 2015.

[9] J. El Yagoubi, G. Lubineau, F. Roger, and J. Verdu, "A fully coupled diffusion--reaction scheme for moisture sorption--desorption in an anhydride-cured epoxy resin," *Polymer (Guildf).*, vol. 53, no. 24, pp. 5582–5595, 2012.

[10] V. A. Guzman and P. Brøndsted, "Effects of moisture on glass fiber-reinforced polymer composites," *J. Compos. Mater.*, vol. 49, no. 8, pp. 911–920, Apr. 2015.

[11] A. Kootsookos and A. P. Mouritz, "Seawater durability of glass- and carbon-polymer composites," *Compos. Sci. Technol.*, vol. 64, no. 10–11, pp. 1503–1511, Aug. 2004.

[12] A. Apicella, R. Tessieri, and C. de Cataldis, "Sorption modes of water in glassy epoxies," *J. Memb. Sci.*, vol. 18, pp. 211–225, Jan. 1984.

[13] J. Zhou and J. P. Lucas, "Hygrothermal effects of epoxy resin. Part I: the nature of water in epoxy," *Polymer (Guildf).*, vol. 40, no. 20, pp. 5505–5512, Sep. 1999.

[14] G. Quino, J. El Yagoubi, and G. Lubineau, "Characterizing the toughness of an epoxy resin after wet aging using compact tension specimens with non-uniform moisture content," *Polym. Degrad. Stab.*, vol. 109, pp. 319–326, Nov. 2014.

[15] G. Quino, "Characterization of fracture toughness of epoxy resin after hygrothermal aging," King Abdullah of Science and Technology, 2013.

[16] J. Zhou and J. P. Lucas, "Hygrothermal effects of epoxy resin. Part II: variations of glass transition temperature," *Polymer (Guildf).*, vol. 40, no. 20, pp. 5513–5522, Sep. 1999.

[17] K. Liao, "In-situ Strength Degradation of Glass Fibers in a Pultruded Composite by Environmental Aging," *J. Mater. Sci. Lett.*, vol. 18, no. 10, pp. 763–765, May 1999.

[18] U. Gaur, C. T. Chou, and B. Miller, "Effect of hydrothermal ageing on bond strength," *Composites*, vol. 25, no. 7, pp. 609–612, Jan. 1994.

[19] H. D. Wagner and A. Lustiger, "Effect of water on the mechanical adhesion of the

glass/epoxy interface," *Composites*, vol. 25, no. 7, pp. 613–616, Jan. 1994.
[20] G. Alawsi, S. Aldajah, and S. A. Rahmaan, "Impact of humidity on the durability of E-glass/polymer composites," *Mater. Des.*, vol. 30, no. 7, pp. 2506–2512, 2009.
[21] D. E. Mouzakis, H. Zoga, and C. Galiotis, "Accelerated environmental ageing study of polyester/glass fiber reinforced composites (GFRPCs)," *Compos. Part B Eng.*, vol. 39, no. 3, pp. 467–475, 2008.
[22] M. J. Adamson, "Thermal expansion and swelling of cured epoxy resin used in graphite/epoxy composite materials," *J. Mater. Sci.*, vol. 15, no. 7, pp. 1736–1745, Jul. 1980.
[23] G. Z. Xiao and M. E. R. Shanahan, "Swelling of DGEBA/DDA epoxy resin during hygrothermal ageing," *Polymer (Guildf).*, vol. 39, no. 14, pp. 3253–3260, Jun. 1998.
[24] K. Derrien and P. Gilormini, "The effect of moisture-induced swelling on the absorption capacity of transversely isotropic elastic polymer--matrix composites," *Int. J. Solids Struct.*, vol. 46, no. 6, pp. 1547–1553, Mar. 2009.
[25] J. E. Shelby, "Introduction to Glass Science and Technology," 2nd ed., Royal Society of Chemistry, 2015.
[26] ASTM International, "ASTM D3039, Standard Test Method for Tensile Properties of Polymer Matrix Composite Materials." ASTM International, West Conshohocken, PA, pp. 1–13, 2008.
[27] ASTM International, "ASTM D2344, Standard Test Method for Short-Beam Strength of Polymer Matrix Composite Materials," *Annual Book of ASTM Standards*, vol. 00, no. Reapproved 2006. West Conshohocken, PA, pp. 1–8, 2011.
[28] G. Quino, A. Pellegrino, V. L. Tagarielli, and N. Petrinic, "Measurements of the effects of pure and salt water absorption on the rate-dependent response of an epoxy matrix," *Compos. Part B Eng.*, vol. 146, pp. 213–221, Aug. 2018.
[29] C. . Buckley, J. Harding, J. . Hou, C. Ruiz, and A. Trojanowski, "Deformation of thermosetting resins at impact rates of strain. Part I: Experimental study," *J. Mech. Phys. Solids*, vol. 49, no. 7, pp. 1517–1538, Jul. 2001.
[30] R. Gerlach, C. R. Siviour, N. Petrinic, and J. Wiegand, "Experimental characterisation and constitutive modelling of RTM-6 resin under impact loading," *Polymer (Guildf).*, vol. 49, no. 11, pp. 2728–2737, 2008.
[31] A. Pellegrino, V. L. Tagarielli, R. Gerlach, and N. Petrinic, "The mechanical response of a syntactic polyurethane foam at low and high rates of strain," *Int. J. Impact Eng.*, vol. 75, pp. 214–221, Jan. 2015.
[32] M. V. Pathan, V. L. Tagarielli, and S. Patsias, "Numerical predictions of the anisotropic viscoelastic response of uni-directional fibre composites," *Compos. Part A Appl. Sci. Manuf.*, vol. 93, pp. 18–32, Feb. 2017.
[33] R. T. Brannan, "Further Evidence Against the Orientation of Structure in Glass Fibers," *J. Am. Ceram. Soc.*, vol. 36, no. 7, pp. 230–231, Jul. 1953.
[34] COMSOL AB, "COMSOL Multiphysics v. 4.4. www.comsol.com." Stockholm, Sweden, 2013.
[35] M. V. Pathan, S. Patsias, J. A. Rongong, and V. L. Tagarielli, "Measurements and predictions of the viscoelastic properties of a composite lamina and their sensitivity to temperature and frequency," *Compos. Sci. Technol.*, vol. 149, pp. 207–219, Sep. 2017.
[36] M. V. Pathan, V. L. Tagarielli, S. Patsias, and P. M. Baiz-Villafranca, "A new algorithm to generate representative volume elements of composites with cylindrical or spherical fillers," *Compos. Part B Eng.*, vol. 110, pp. 267–278, Feb. 2017.
[37] Dassault Systèmes, *Abaqus version 6.14 (Computer application)*. ABAQUS Inc.,

2014.
[38] I. M. Ward and J. Sweeney, *An introduction to the mechanical properties of solid polymers*, 2nd ed. Wiley, 2004.
[39] C. J. Tsenoglou, S. Pavlidou, and C. D. Papaspyrides, “Evaluation of interfacial relaxation due to water absorption in fiber–polymer composites,” *Compos. Sci. Technol.*, vol. 66, no. 15, pp. 2855–2864, Dec. 2006.